

Absence of Berezinskii-Kosterlitz-Thouless phase transition in two-dimensional Axial-Next-Nearest-Neighbor Ising model

René Derian¹, Andrej Gendiar², and Tomotoshi Nishino³

¹*Institute of Physics, Slovak Academy of Sciences, SK-845 11 Bratislava, Slovakia*

²*Institute of Electrical Engineering, Slovak Academy of Sciences, SK-841 04 Bratislava, Slovakia and*

³*Department of Physics, Faculty of Science, Kobe University, Kobe 657-8501, Japan*

(Dated: January 15, 2019)

The axial next-nearest-neighbor Ising model is studied in two dimensions at finite temperature using the density matrix renormalization group. The model exhibits only one phase transition of the second-order between the antiphase and the paramagnetic phase and no Berezinskii-Kosterlitz-Thouless phase transition is observed. We conclude absence of incommensurate phase in the model.

PACS numbers: 64.70.Rh, 75.10.Hk, 75.40.Mg, 02.70.-c

Periodically modulated structures may occur in a wide range of physical systems. As examples of such systems, $\text{La}_6\text{Ca}_8\text{Cu}_{24}\text{O}_{41}$ and $\text{Ca}_2\text{Y}_2\text{Cu}_5\text{O}_{10}$ are well known [1, 2], where spins of the copper atoms interact ferromagnetically between the neighboring sites along the CuO_2 chains and antiferromagnetically between the next-nearest-neighboring ones. A phase transition of commensurate-incommensurate type was observed in these systems. Another example is cerium antimonide (CeSb) [3] which has a nontrivial phase diagram and which shows modulated spin patterns with various periodicities. In some ferroelectric materials, such as NaNO_3 , the modulated phases are present between the ferroelectric low-temperature state and the paraelectric high-temperature one [4, 5].

Physical properties of magnetically modulated structures can be described by simplified models with competing interactions. One of the simplest examples is the so-called axial next-nearest-neighbor Ising (ANNNI) model, which contains ferromagnetic coupling between nearest-neighbor spin pairs and antiferromagnetic one between next-nearest-neighbor spin pairs in a preferred direction. [6]. Several analytical methods have been developed to study the phase diagram of the ANNNI model in two dimensions. For instance, the free-fermion approximation treats domain walls running along the chain direction [7]. Müller-Hartmann-Zittartz approach assumes existence of the domain wall in the perpendicular direction to the axial one [8]. A detailed survey of earlier works on this topic has been reviewed by Selke [6] while the recent progress can be found in Refs. 9, 10, 11.

Although the topology of the phase diagram of the two-dimensional (2D) ANNNI model has been widely accepted, the position of the Berezinskii-Kosterlitz-Thouless (BKT) transition [12, 13] is highly dependent on the way of analysis. Significant contribution came later when the ANNNI model was studied by means of Monte Carlo simulations. Substantially lower temperatures of the BKT transition were estimated by Sato and Matsubara [14]. Later, Shirahata and Nakamura applied the non-equilibrium relaxation method for much larger

systems [9]. Assuming the presence of the BKT transition, they estimated two critical temperatures bordering the incommensurate phase and found them almost identical. They speculated that successive phase transitions may occur within an infinitesimally narrow temperature region.

The aim of our study is to clarify the phase structure of the 2D ANNNI model. For this purpose we employ the density matrix renormalization group (DMRG) [15, 16, 17] method and carry out a precise analysis of the domain-wall free energy around the phase transition. As shown in the following, we observe only one phase transition of the second order between the antiphase and the paramagnetic phase. Our result contradicts to all previous conjectures [6] since it excludes the BKT transition. Table I summarizes these above-stated situations and we explain the meaning of κ and T_c in the following.

We consider the 2D ANNNI model described by the Hamiltonian

$$\mathcal{H} = -J_1 \sum_{i,j} \sigma_{i,j} (\sigma_{i+1,j} + \sigma_{i,j+1}) - J_2 \sum_{i,j} \sigma_{i,j} \sigma_{i+2,j} \quad (1)$$

on a square lattice with the size $L \times \infty$, where the index i runs from 1 to L toward the axial direction. The Ising spins $\sigma_{i,j} = \uparrow$ or \downarrow interact ferromagnetically ($J_1 > 0$) between the nearest neighbors and antiferromagnetically

TABLE I: List of critical temperatures T_c (the second-order) and T_{BKT} (Berezinskii-Kosterlitz-Thouless) at $\kappa = 0.6$ obtained by various methods.

Method used	T_c	T_{BKT}
Müller-Hartmann-Zittartz [8]	1.09	missing
Phenomenological renormalization [18]	1.05	1.35
Saqi and McKenzie [19]	1.05	1.40
Cluster variation method [20]	0.91	1.64
Cluster heat bath method [14]	0.91	1.16
Free-fermion approximation [7]	0.907	1.20
Non-equilibrium Relaxation [9]	0.89(2)	0.895(25)
DMRG (this work)	0.907	—

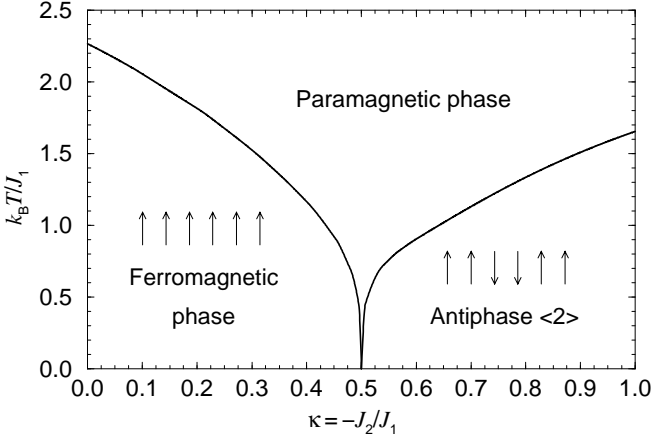


FIG. 1: The calculated phase diagram.

$(J_2 < 0)$ between the next-nearest neighbors. We define $\kappa = -J_2/J_1$ that measures degree of the frustration.

Consider a transfer matrix $\mathcal{T}_L[\sigma'|\sigma]$ that connects two adjacent spin rows $[\sigma'] \equiv \{\sigma_{1,j}, \sigma_{2,j}, \dots, \sigma_{L,j}\}$ and $[\sigma] \equiv \{\sigma_{1,j-1}, \sigma_{2,j-1}, \dots, \sigma_{L,j-1}\}$. We drop out the indices j and $j-1$ for simplicity in the following. Without loss of generality, the transfer matrix can be written in the product of the overlapped weights

$$\mathcal{T}_L[\sigma'|\sigma] = \prod_{i=1}^{L-2} W_B(\sigma'_i \sigma'_{i+1} \sigma'_{i+2} | \sigma_i \sigma_{i+1} \sigma_{i+2}), \quad (2)$$

where $W_B(\sigma'_i \sigma'_{i+1} \sigma'_{i+2} | \sigma_i \sigma_{i+1} \sigma_{i+2})$ is the local Boltzmann weight associated with the Hamiltonian \mathcal{H} [10, 21]. The DMRG is employed to solve the eigenvalue problem

$$\sum_{[\sigma]} \mathcal{T}_L[\sigma'|\sigma] \Psi_L[\sigma] = \lambda_L(T) \Psi_L[\sigma'] \quad (3)$$

with $\lambda_L(T)$ being the largest eigenvalue of the transfer matrix and $\Psi_L[\sigma]$ the corresponding eigenvector. We employ two different boundary conditions: the parallel ones ($\sigma_1 = \uparrow$ and $\sigma_L = \uparrow$) and the antiparallel ones ($\sigma_1 = \uparrow$ and $\sigma_L = \downarrow$) for which we calculate the largest eigenvalues $\lambda_L^{\uparrow\uparrow}(T)$ and $\lambda_L^{\uparrow\downarrow}(T)$, respectively. For the visualization of the spin modulation, we directly calculate the local magnetization

$$\langle \sigma_i \rangle = \frac{\sum_{[\sigma]} \Psi_L[\sigma] \sigma_i \Psi_L[\sigma]}{\sum_{[\sigma]} \Psi_L[\sigma] \Psi_L[\sigma]} \quad (4)$$

as a function of position i during the DMRG's finite-size sweep in DMRG [15]. We keep at most $m = 70$ block-spin states and vary the lattice size from $L = 38$ to $L = 118$. Note that under these conditions, the accuracy of the numerical calculations is kept within the density matrix truncation error [15, 16, 17] $\varepsilon \leq 10^{-13}$. We use

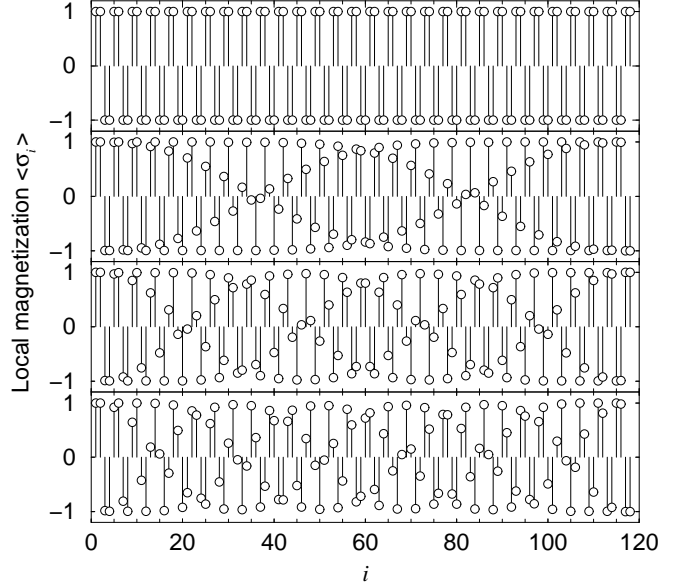


FIG. 2: The local magnetization $\langle \sigma_i \rangle$ calculated for $L = 118$ ($i = 1, 2, \dots, 118$) with parallel and antiparallel boundary conditions.

dimensionless units and set $k_B = J_1 = 1$ throughout this article.

Figure 1 shows the calculated phase diagram. At higher temperatures, thermal fluctuations prevail over any magnetic structures and the paramagnetic phase is realized. There is a second order transition from the ferromagnetic state to the paramagnetic one if $\kappa < 0.5$. [6, 7, 8, 9, 14, 18, 19, 20]. When κ is larger than 0.5, the antiphase structure $\{\dots \uparrow\uparrow\downarrow\downarrow \dots\}$ is realized at low temperatures. In the following, we focus on analysis of the model at $\kappa = 0.6$ in detail.

Figure 2 shows the local magnetization $\langle \sigma_i \rangle$ at $\kappa = 0.6$ under and over a transition temperature $T_c \approx 0.91$ (see Table I) that we will determine more precisely. The complete antiphase structure $\{\uparrow\uparrow\downarrow\downarrow\}$ is observed at $T = 0.88$ if the parallel boundary conditions are imposed (the uppermost) and a twisted pattern created by a running domain wall is observed for the antiparallel conditions (the second from top). The remaining two panels display $\langle \sigma_i \rangle$ at $T = 0.93$, where a modulated structure is present for the parallel conditions (the third panel) and the antiparallel ones (the fourth). Note that the modulation period depends on the applied boundary conditions.

For the purpose of characterizing the spin modulation, we introduce the “domain-wall free energy” [22]

$$\mathcal{F}_{DW}(T, L) = -k_B T \ln \frac{\lambda_L^{\uparrow\uparrow}(T)}{\lambda_L^{\uparrow\downarrow}(T)}, \quad (5)$$

which represents the sensitivity of the free energy per lattice raw to the boundary conditions. In the antiphase

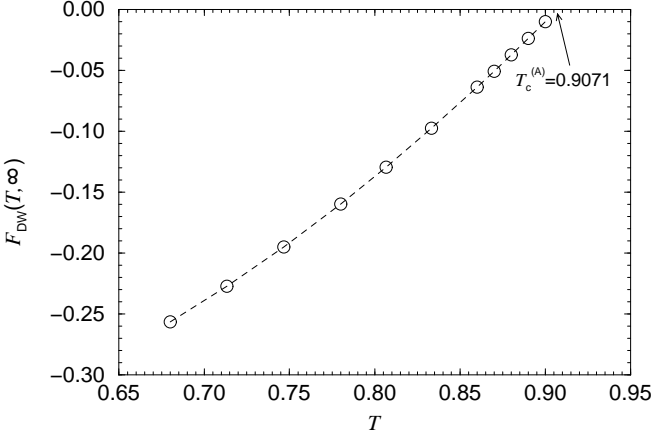


FIG. 3: The stationary domain-wall energy $\mathcal{F}_{\text{DW}}(T, \infty)$ vs T at $\kappa = 0.6$.

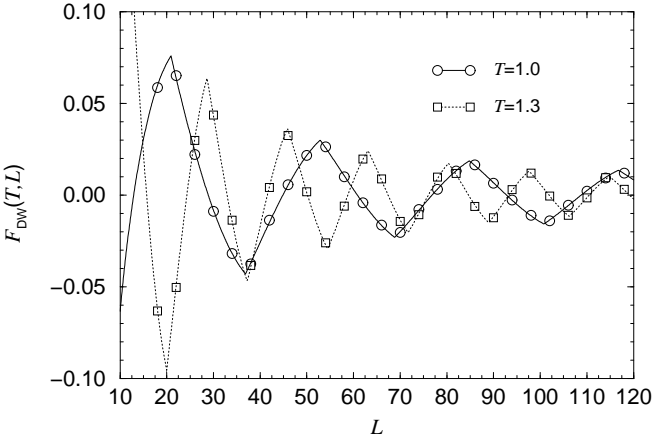


FIG. 4: The domain-wall free energy with respect to size L at $T = 1.0$ (circles) and $T = 1.3$ (squares) for $\kappa = 0.6$. The saw-like fitting functions are given by Eq. (8).

region, $\mathcal{F}_{\text{DW}}(T, L)$ exhibits the L dependence

$$\mathcal{F}_{\text{DW}}(T, L) \sim \mathcal{F}_{\text{DW}}(T, \infty) + c(T)L^{-2}, \quad (6)$$

where $c(T)$ is a fitting parameter and the ‘stationary’ domain-wall energy $\mathcal{F}_{\text{DW}}(T, \infty)$ can be easily evaluated. Figure 3 shows the dependence of $\mathcal{F}_{\text{DW}}(T, \infty)$ with respect to T . The domain-wall free energy vanishes at critical temperature $T_c^{(\text{A})} = 0.907$; the superscript (A) stands for the antiphase region.

A detailed analysis of the $\mathcal{F}_{\text{DW}}(T, L)$ is required in the higher temperature region ($T > T_c$). The typical L -dependence of $\mathcal{F}_{\text{DW}}(T, L)$ is depicted in Fig. 4. The saw-like structure is naturally explained from the wave number $q(T)$ in modulation pattern in the limit $L \rightarrow \infty$. If L is finite, the boundary conditions force the system to have a modified wave number $q'(T)$, which is quantized

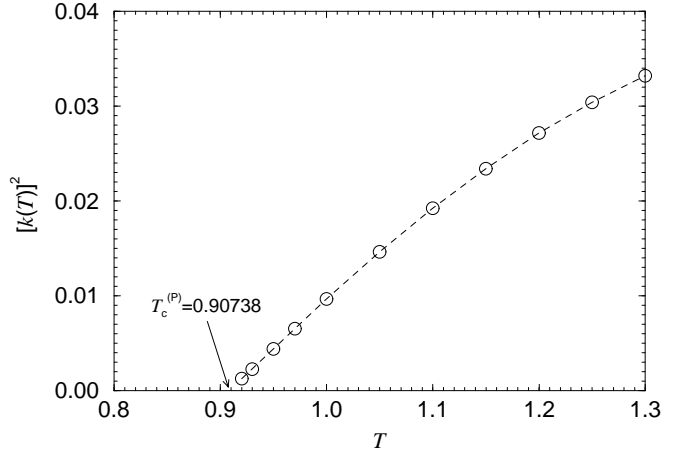


FIG. 5: Behavior of the wave number $[k(T)]^2 = [q(T) - \pi/2]^2$.

as

$$\begin{aligned} q'_{\uparrow\uparrow}(T) &= 2\pi m/(L - \ell), \\ q'_{\uparrow\downarrow}(T) &= 2\pi(m + 1)/(L - \ell), \end{aligned} \quad (7)$$

respectively, for the parallel and the antiparallel conditions, where m is an appropriate integer and ℓ is an offset. As a consequence of the ‘forced’ shift in the wave number, a small increase of the free energy per site occurs and is proportional to $[q(T) - q'_{\uparrow\uparrow}(T)]^2$ and $[q(T) - q'_{\uparrow\downarrow}(T)]^2$ if higher-order corrections are omitted. Paying attention to the quantization condition in Eq. (7) and subtracting $\mathcal{F}_{\uparrow\uparrow}(T, L) = -k_B T \ln \lambda_L^{\uparrow\uparrow}(T)$ from $\mathcal{F}_{\uparrow\downarrow}(T, L) = -k_B T \ln \lambda_L^{\uparrow\downarrow}(T)$, we obtain the saw-like dependence in $\mathcal{F}_{\text{DW}}(T, L)$ with respect to L shown in Fig. 4. For the quantitative determination of $q(T)$, we employ a fitting function of the form

$$\mathcal{F}_{\text{DW}}(T, L) = \frac{ae^{-dL}}{L} \{ |\cos(kL + \varphi)| - |\sin(kL + \varphi)| \} \quad (8)$$

that contains four temperature dependent parameters: a is an amplitude, φ is the phase offset related to ℓ in Eq. (7), d is a damping, and $k \equiv k(T) = q(T) - \pi/2$ represents a change of the wave number $q(T)$ from the antiphase wave number $\pi/2$ [23]. At $T > T_c$ we found no singular behavior of the fitting parameters. In Fig. 5, we plot $[k(T)]^2$ as a function of temperature T . Performing the extrapolation of $k(T) \rightarrow 0$, we obtain the critical temperature $T_c^{(\text{P})} = 0.907$ within the paramagnetic region. This result is in accordance with the previous $T_c^{(\text{A})}$.

As an independent analysis, we calculate $\mathcal{F}_{\text{DW}}(T, L)$ as a function of T at $\kappa = 0.6$ (see Fig. 6.) Again, we obtain the saw-like dependence of $\mathcal{F}_{\text{DW}}(T, L)$ which rapidly decays in higher temperature region. Extrapolation to the large L limit should be considered in order to conclude that the paramagnetic phase is realized above T_c .

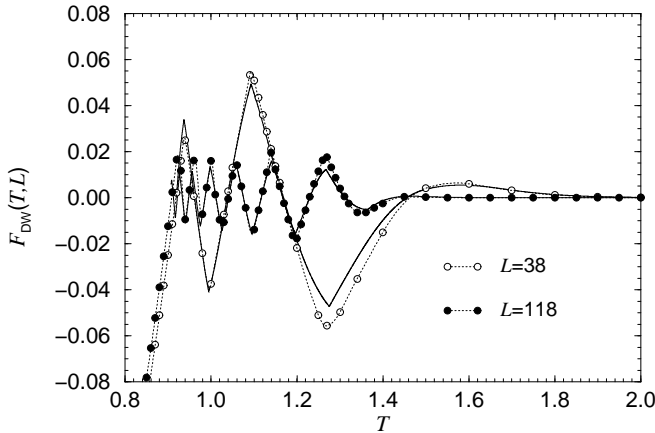


FIG. 6: Dependence of $\mathcal{F}_{\text{DW}}(T, L)$ on temperature T at $\kappa = 0.6$. The symbols connected by the dotted curves represent our numerical data and the full curves reconstruct $\mathcal{F}_{\text{DW}}(T, L)$ from Eq. (8).

For this purpose we check the agreement of the obtained $\mathcal{F}_{\text{DW}}(T, L)$ with the fitting function in Eq. (8). As shown in Fig. 6 a good agreement is found between numerical data (the circles) and the fitting function (the full curves) when the previously obtained temperature dependent parameters a , k , φ , and d are substituted to Eq. (8). Now, we focus on the ‘first’ zero-crossing point from the low-temperature region. The wave number $q(T)$ starts to deviate from $\pi/2$ at the critical temperature T_c and $\mathcal{F}_{\text{DW}}(T, L)$ becomes zero if

$$[q(T) - \pi/2]L = k(T)L = \pi/2 \quad (9)$$

is satisfied. The zero-crossing temperature, say $T_0(L)$, must give the true transition temperature in the limit $L \rightarrow \infty$. Remember that in Fig. 5 we observe $k(T) \propto \sqrt{T - T_c}$. This implies that $\sqrt{T - T_0(L)} \propto L^{-1}$ holds. In order to confirm this relation, we plot Fig. 7, where we show the linearity between relative temperature $t = [T_0(L) - T_0(\infty)]/T_0(\infty)$ and L^{-2} where $T_0(\infty)$ for each κ is appropriately chosen so that the best linearity is realized. It should be noted that the critical exponent $\nu = 0.5$ is resulted and it refers to the scaling relation $t \propto L^{-1/\nu}$ which is a consequence of the divergence of the correlation length at T_c [21]. We determined $T_0(\infty) = 0.907$ at $\kappa = 0.6$ and the result is in accordance with the $T_c^{(\text{A})}$ from Fig. 3 and $T_c^{(\text{P})}$ from Fig. 5. If $T_c^{(\text{A})} = T_c^{(\text{P})} = T_0(\infty)$ is assumed for other $\kappa > 0.5$, we obtain $T_c = 1.335$ at $\kappa = 0.8$, and $T_c = 1.654$ at $\kappa = 1.0$.

In conclusion, we have applied DMRG to the 2D ANNNI model. We observed the second-order phase transition only, which is detected by the scaling analysis from both the low and the high temperature regions. Regular behavior of the fitting parameters that appears in the domain-wall free energy supports that there is no Berezinskii-Kosterlitz-Thouless phase transition in the

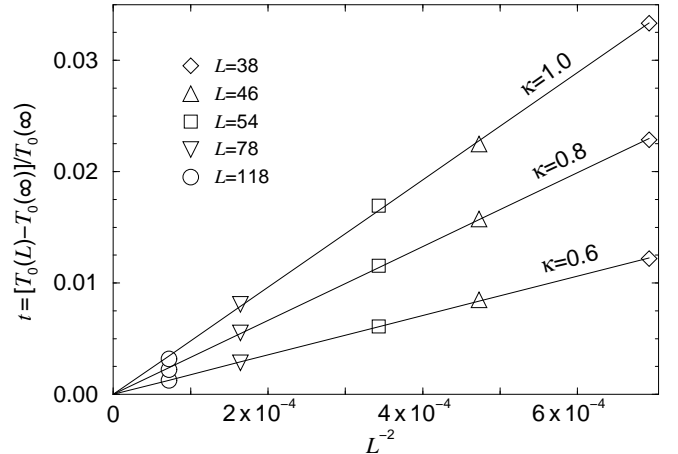


FIG. 7: The scaling behavior t with respect to L^{-2} for $\kappa = 0.6$, $\kappa = 0.8$, and $\kappa = 1.0$.

model. Hence, the absence of the incommensurate phase in the 2D ANNNI model is concluded.

This work is supported by the VEGA grants No. 2/3107/23 and No. 2/3118/23, and the Grant-in-Aid for Scientific Research from Ministry of Education, Science, Sports and Culture (No. 17540327).

- [1] M. Matsuda, K. Katsumata, T. Yokoo, S. M. Shapiro, and G. Shirane, Phys. Rev. B **54**, R15626 (1996).
- [2] H. F. Fong, B. Keimer, A. Hayashi, and R. J. Cava, Phys. Rev. B **59**, 6873 (1999).
- [3] J. Rossat-Mignot, P. Burlet, J. Villain, H. Bartholin, W. Tcheng-Si, D. Florence, and O. Vogt, Phys. Rev. B **16**, 440 (1977).
- [4] Y. Yamada, I. Shibuya, and S. Hoshino, J. Phys. Soc. Jpn. **18**, 1594 (1963).
- [5] V. Massida and C. Mirasso, Phys. Rev. B **40**, 9327 (1989).
- [6] W. Selke, Phys. Rep. **170**, 213 (1988).
- [7] J. Villain and P. Bak, J. Phys. (Paris) **42**, 657 (1982).
- [8] J. Kroemer and W. Pesch, J. Phys. A **15**, L25 (1982).
- [9] T. Shirahata and T. Nakamura, Phys. Rev. B **65**, 024402 (2002).
- [10] A. Gendiar and T. Nishino, Phys. Rev. B **71**, 024404 (2005).
- [11] A. Gendiar and A. Šurda, J. Phys. A: Math. Gen. **33**, 8365 (2000).
- [12] V. Berezinskii, Sov. Phys. JETP **34**, 610 (1972).
- [13] J. Kosterlitz and D. Thouless, J. Phys. C **6**, 1181 (1973).
- [14] A. Sato and F. Matsubara, Phys. Rev. B **14**, 10316 (1999).
- [15] S. R. White, Phys. Rev. Lett. **69**, 2863 (1992).
- [16] T. Nishino, J. Phys. Soc. Jpn. **64**, 3598 (1995).
- [17] U. Schollwoeck, Rev. Mod. Phys. **77**, 259 (2005).
- [18] M. Grynberg and H. Ceva, Phys. Rev. B **36**, 7091 (1987).
- [19] M. Saqi and D. McKenzie, J. Phys. A **20**, 471 (1987).
- [20] Y. Murai, K. Tanaka, and T. Morita, Physica A **217**, 214 (1995).

- [21] M. N. Barber, *Finite-size Scaling* (Academic Press, 1983).
- [22] H. Richards, M. Novotny, and P. Rikvold, Phys. Rev. B **48**, 14584 (1993).
- [23] We show the details elsewhere.